

DR4907-1213-PRFSS-001

**Centrifugal Compressor Meanline
Design Using Real Gas Properties**

by

Sukhveer S. Sanghera

Department of Mechanical and Aerospace Engineering
Carleton University
Ottawa, Ontario, Canada

April 2013

Abstract

When designing a centrifugal compressor it is a good idea to investigate a large number of proposed configurations before moving ahead with a specific design. A reasonably accurate performance analysis has been developed by turbomachinery aerodynamicists in order to meet this demand, often referred to as meanline analysis. This report describes a method for using meanline analysis to determine the performance of compressors operating with non-ideal working fluids, and is intended to aid students in the design of the 250kW supercritical carbon dioxide Brayton cycle being created at Carleton University. A Fortran code was developed to automate the analysis and encorporate gas equations of state from REFPROP 9.0 and benchmark testing on the Eckardt rotor is used to validate the accuracy of the code.

Acknowledgements

I would like to thank Professor Sjolander for his guidance and leadership over the course of the project and the performance group for being awesome.

Contents

1	Introduction	1
2	Methodology	3
2.1	Fundamentals	4
2.1.1	Inlet Guide Vanes	5
2.1.2	Impeller	5
2.1.3	Diffuser	6
2.1.4	Volute	6
2.1.5	Definition of the Meanline	6
2.2	Gas Equations of State	7
2.3	Meanline Analysis of a Centrifugal Compressor	8
2.3.1	Impeller Inlet	9
2.3.2	Impeller Outlet	11
2.3.3	Internal Losses	14
2.3.4	Slip Factor	17
2.3.5	Parasitic Losses	19
2.3.6	Diffuser Losses	20
2.3.7	Volute Losses	21
2.3.8	Compressor Outlet of Performance Prediction	21
3	Results	23
3.1	CCMD Benchmark Testing	23
4	Conclusion	26
4.1	Recommendations	26
4.2	Final Remarks	27

List of Tables

3.1	Eckardt O-Rotor Dimensions	24
3.2	Eckardt O-Rotor Performance. CCMD vs. Experimental Data . . .	24

List of Figures

2.1	Single stage centrifugal compressor in the r- plane.	4
2.2	Single stage centrifugal compressor in the r-Z plane.	4
2.3	Impeller used on a gas turbine engine.	5
2.4	Errors of using ideal gas approximation near CP[6].	7
2.5	Algorithm flowchart of the Fortran program.	8
2.6	H-S diagram at the impeller inlet.	9
2.7	Impeller inlet velocity triangle.	10
2.8	H-S Diagram at the rotor outlet (initial estimate).	11
2.9	Rotor outlet velocity triangle.	13
2.10	Non-uniform velocities at impeller outlet (Johnston and Dean, 1966).	16
2.11	Impeller outlet velocity triangle with slip (Sjolander,[4]).	18
2.12	Full compressor performance H-S diagram.	22
3.1	The Eckardt O-Rotor (Japikse and Baines, 1997).	23

Nomenclature

0	Total conditions
1	Impeller inlet
2	Impeller outlet
3	Diffuser inlet
4	Diffuser outlet
a	Axial component
b	Blade meanline path
BL	Blade loading
cl	Clearance
DF	Disc friction
h	Hub
inc	Incidence
LL	Leakage loss
m	Meanline
mix	Mixing
r	Radial
RC	Recirculation
s	Shroud
SF	Skin friction
U	Tangential component
W	Relative component

\dot{m}	Mass flow rate [kg/s]
η	Efficiency
μ	Dynamic viscosity [Pa s]
ρ	Density [kg/m^3]
σ	Slip factor
C_f	Skin friction coefficient
A	Area [m^2]
b	Passage width [m]
C	Absolute velocity [m/s]
D	Diameter [m]
h	Enthalpy [J/kg]
L	Length [m]
P	Pressure [kPa]
PR	Pressure ratio [total-total]
r	Radius [m]
s	Tip clearance [mm]
t	Blade thickness [m]
U	Blade circumferential speed [m/s]
W	Relative velocity [m/s]
Z	Number of Blades
	Rotational Speed [rad/s]

Section 1

Introduction

The desire to increase the pressure in a flow is seen in many industries. For example, performance vehicles use turbochargers to force more air into the engine which increases efficiency, rockets use it to decrease the initial pressurization required in the fuel tanks which reduces launch weight, and gas turbine generators use it to drive the flow through the cycle which, in turn, creates electricity. Typically, the most common way of increasing the pressure in a flow is by increasing it's kinetic energy and converting this kinetic energy into pressure energy. Imagine passing the flow through something rotating at very high speeds, the faster you spin the flow, the more kinetic energy it will gain, so the more pressure you can gain. This is the basis for how both axial and centrifugal compressors work (and vice versa, turbines, which instead extract energy from a flow).

However, predicting how the flow behaves through these rotating machines (turbomachinery) is very non intuitive, making it difficult to engineer a design with reasonable accuracy. Thankfully, the contributions of many turbomachinery aerodynamicists over the years has led to a simplified method (often referred to as meanline analysis) of predicting how the flow behaves through turbomachinery. Meanline analysis is especially useful in the early stages of design because many iterations may be required and the analysis can be computed fairly quickly. Another important development for turbomachinery design is the tabulation of a wide variety of fluids over an extended range of operating conditions. This has led to the discovery of certain working fluids which can increase the efficiency of turbomachinery at certain conditions. Making it desirable to extend the capability of meanline analysis to capture these effects.

The meanline analysis method was used for the design of the 250 kWe pilot scale SCO_2 Brayton Cycle test loop being developed at Carleton University which features a single stage centrifugal compressor. The purpose of this project is to conduct studies on high-efficiency power conversion systems based on SCO_2 cycles. The plant is designed so that the SCO_2 flowing through the compressor is just above the critical point, where the fluid behaves like a gas (expanding to fill it's container) and has the density similar to that of a liquid. This makes the fluid

easier to compress which reduces the required work input and therefore increases the overall plant efficiency. It also allows for high efficiencies to be obtained at relatively low temperatures of around 600°C, whereas conventional Brayton Cycles would have to operate at much higher temperatures of approximately 900°C to achieve the same efficiencies. For more information on SCO_2 cycles see [1].

This report is intended to provide an overview of a meanline analysis method which uses NIST REFPROP to obtain thermodynamic properties of a wide range of fluids with an extended range of operating conditions, this is explained in detail in Section 2. The analysis was compared to experimental data to test the accuracy and is presented in Section 3. In addition, Section 4 contains a study of the errors involved when using the ideal gas approximation for fluids opposed to using REFPROP. Finally, recommendations for improvement in the analysis and a conclusion is provided in Section 5. Also, because of the large amounts of iteration required in the preliminary design phase of centrifugal compressors, and the need to integrate REFPROP into the analysis, the meanline analysis method was implemented into a Fortran code.

Section 2

Methodology

The simplified performance analysis of centrifugal compressors begins by assuming the flow along the mean streamline represents the bulk flow properties through the compressor. Next, the laws of conservation of mass and energy in the rotating frame of reference which leads to the fundamental law of turbomachinery, also known as the Euler turbine equation. The Euler equation is given as:

$$h_{02} - h_{01} = \omega(r_2 C_{W2} - r_1 C_{W1}) \quad (2.1)$$

However, fluids behave very differently depending on their temperature and pressure, so it is necessary to incorporate gas equations of state which can predict the properties of the fluid in the conditions it will be operating in. The current “gold-standard” for gas equations of state for a wide range of fluids is available from the National Institute of Standards and Technology (NIST) [5]. This data, referred to as the REference fluid thermodynamic and transport PROPERTIES database (REF-PROP), is available in many formats, including Fortran code. Now it is possible determine things like the enthalpy of the fluid at given temperatures and pressures.

Next, non-dimensionalized loss correlations are obtained from the published data of various researchers. These independant discoveries have provided explainations for phenomenom that occur within centrifugal compressors, this includes incidence losses, blade loading losses, skin friction losses, clearance losses, mixing losses, and various parasitic losses. Loss correlations are the key to simplifying a complex three dimensional performance analysis of centrifugal compressors to one dimension, and have been validated for a full range of machine sizes and operating conditions.

There exists many loss correlations which each have their advantages and disadvantages for certain sizes and speeds of turbomachinery. This makes it desirable to find an optimum set of loss correlations which can predict the performance of a full range of centrifugal compressors. A set of loss correlations provided by Oh. et. al. [2] was chosen in this analysis, however other alternative methods do exist, i.e. Aungier [3].

2.1 Fundamentals

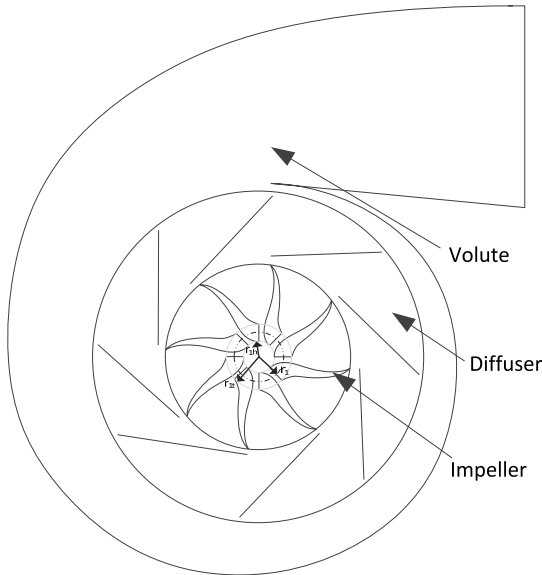


Figure 2.1: Single stage centrifugal compressor in the r - plane.

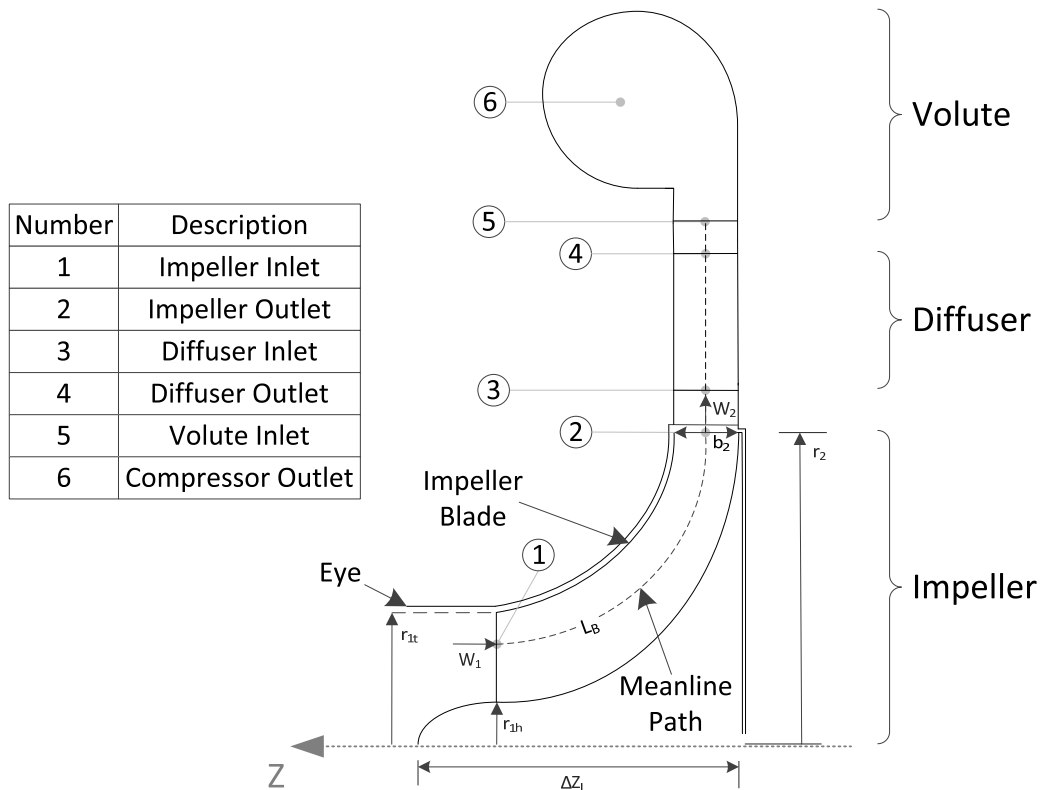


Figure 2.2: Single stage centrifugal compressor in the r - Z plane.

A single stage centrifugal compressor consists of three parts: a rotating impeller which imparts kinetic energy to the flow (also referred to as the rotor), a stationary diffuser which converts the kinetic energy into a pressure increase, and a volute which smoothly discharges the flow.

2.1.1 Inlet Guide Vanes

The flow enters the compressor through the inlet eye and into the rotating impeller. Most machines have a flow entering the impeller in the axial direction, however for some, it is desireable to enter at some angle. This can be achieved through the use of inlet guide vanes which impart an inlet swirl angle (α_1) to the flow.

2.1.2 Impeller

An impeller is used to rotate the fluid and impart kinetic energy to the fluid. There are two types of impellers, shrouded and unshrouded. Figure 2.3 shows an unshrouded impeller used on a gas turbine engine (which would operate inside a stationary casing).



Figure 2.3: Impeller used on a gas turbine engine.

Shrouded impellers are used when it becomes difficult to keep a tight clearance between casing walls and impeller blades, this is true in multistage engines.

2.1.3 Diffuser

The conversion of kinetic energy to pressure energy can be achieved through many different arrangements. This has led to various types of diffusers, such as vaneless, vaned, pipe diffusers, etc. However, because of purpose of developing this code for the gas turbine project, a full diffuser analysis will not be included. Instead, a loss factor can be input by the user depending on the type of diffuser and volute arrangement which may be chosen later on.

2.1.4 Volute

Volutes are used to smoothen out the flow before entering the pipe or whatever is seen after the compressor. There will also be some frictional losses in the volute depending on the design which is used, and like the diffuser, a simple loss factor will be used for the purposes of this analysis.

2.1.5 Definition of the Meanline

The meanline path of the flow, sometimes referred to as the mean streamline, or meridional path is determined as the root mean square value between the hub radius and shroud radius of the blade, or mathematically,

$$r_m = \sqrt{\frac{1}{2}(r_s)^2 + \frac{1}{2}(r_h)^2} \quad (2.2)$$

This equation can be applied at any point along the flow to determine the location of the meanline path. An estimate of the length of the vane along the meanline path is provided by Sjolander [4].

$$L_b = (\Delta Z - \frac{b_2}{2}) + \frac{1}{2} \left(\frac{D_2 - D_1}{\cos(\beta'_2)} \right) \quad (2.3)$$

Where L_B is the length of the vane along the mean camberline, b_2 is the width of the opening at the impeller outlet and β'_2 is the impeller outlet metal angle. Figure 2.2 shows the meanline path through the impeller and diffuser.

2.2 Gas Equations of State

The thermodynamic properties of all fluids depend on intermolecular forces and molecule sizes. For different temperatures and pressures of a fluid, the molecules will be moving at different speeds and have different momentum. This will have an effect on thermodynamic properties of that fluid such as its density and heat capacity.

However, for some fluids (i.e. air, carbon dioxide, oxygen, and noble gases) there exists a range of temperatures and pressures where these forces are negligible with change in pressure, typically where spacing between molecules are large such as at low pressures, or at very low temperatures intermolecular forces start coming into effect again. If a fluid is operating in these conditions it is said to be an “ideal gas” because density stays fairly constant (referred to as incompressible) and there exists a simplified set of equations of state for determining the fluid thermodynamic properties.

Wherever the ideal gas approximation is invalid (i.e. very high pressures or very low temperatures) the ideal gas equations of state which are used in most turbomachinery analyses become invalid. REFPROP contains curve fits for the tabulated data which can be utilized through the Fortran source code files provided by NIST. Because the nature of these equations of state being obtained through experiment and not using any approximations, they are valid for all industrial operating conditions [5], regardless of whether it is in the ideal gas region or not. This is useful for the case of supercritical carbon dioxide which is operating above the critical point and exhibits highly non-ideal behavior through the compressor.

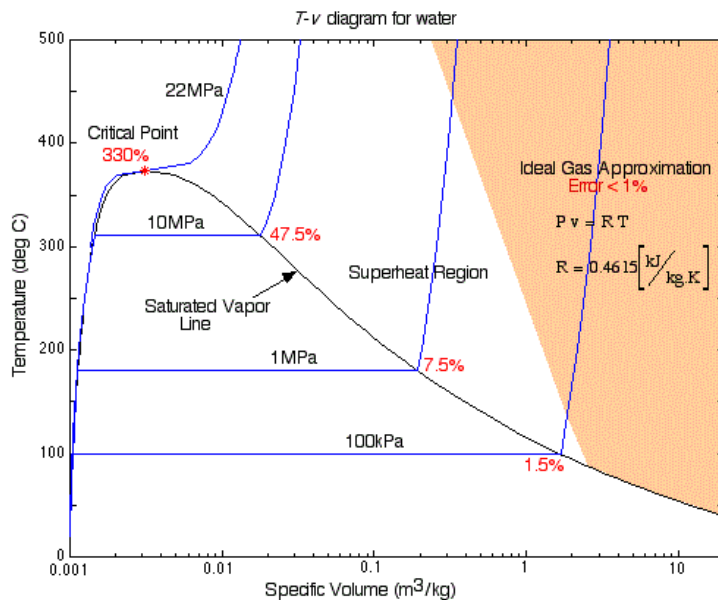


Figure 2.4: Errors of using ideal gas approximation near CP[6].

2.3 Meanline Analysis of a Centrifugal Compressor

An overview of the performance prediction of centrifugal compressors in the order it was coded into Fortran is displayed in Figure 2.5. Numbering stations used throughout the analysis follows what is seen in Figure 2.2.

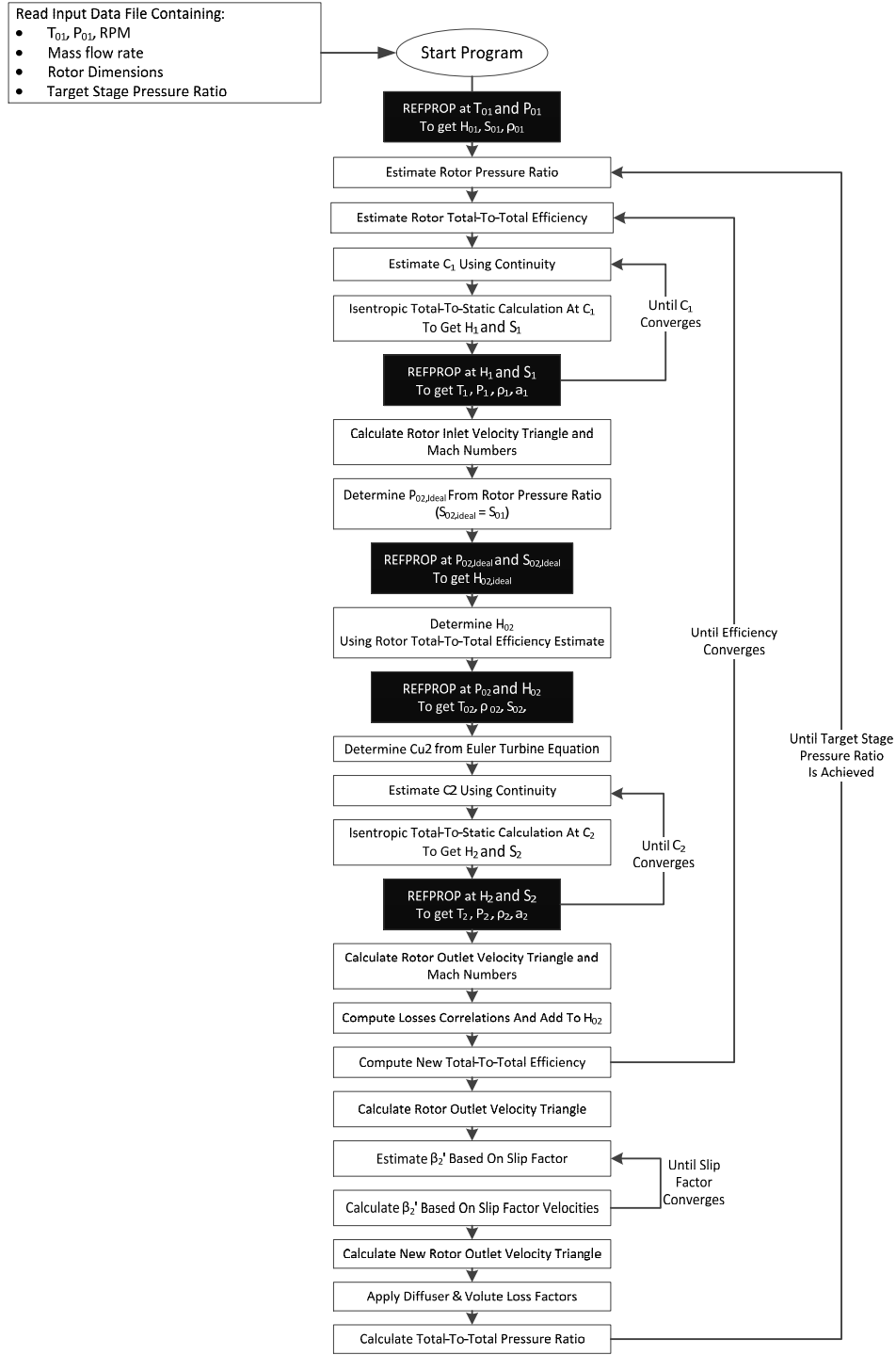


Figure 2.5: Algorithm flowchart of the Fortran program.

2.3.1 Impeller Inlet

The known conditions at the impeller inlet are the total temperature, total pressure, mass flow rate, rotational speed of the rotor, and inlet swirl angle. Typically, two fluid properties are needed in order to determine all other thermodynamic properties using gas equations of state in REFPROP, so from the total temperature and pressure REFPROP returns the total density, total enthalpy, and total entropy. Also, from the mass flow rate, the axial velocity of the flow can be determined using the conservation of mass (also referred to as continuity).

$$\dot{m} = \rho_1 A_1 C_{a1} = \rho_1 A_1 C_1 \cos\alpha_1 \quad (2.4)$$

Where the area of the inlet is given by:

$$A_1 = \pi(r_{1s})^2 - \pi(r_{1h})^2 \quad (2.5)$$

The inlet swirl angle is defined, so there exist two equations and 3 unknowns, the absolute velocity, the axial velocity, and the static density at the inlet. These can be obtained using the total conditions and iteration as follows:

- Use the total density as a first estimate for ρ_1
- Rearrange equation 2.4 and solve for C_1
- Compute the static enthalpy using an isentropic total-to-static process (Fig. 2.6)
- Call REFPROP with the static enthalpy and entropy to determine the ρ_1
- Update the first estimate of ρ_1 and continue this process until convergence

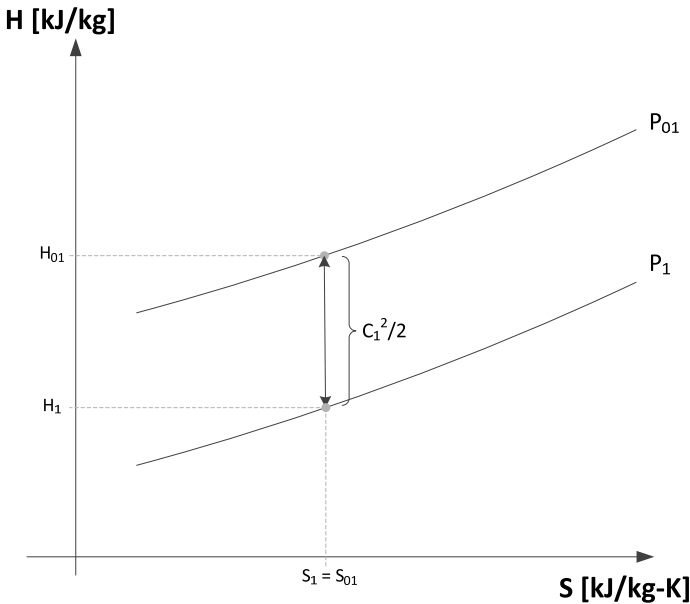


Figure 2.6: H-S diagram at the impeller inlet.

Now the values of C_1 , C_{a1} , α_1 , and U_1 (determined from the rotational speed) are known, so the full velocity triangle at the impeller inlet can be constructed using trigonometry. It is important to note that the angles in velocity triangles are different across literature depending on which axis they are taken from. There is no correct convention, but once one is selected, it is important to stick with it. The convention used in this analysis follows that used by Sjolander [4] and is shown in Figure 2.7.

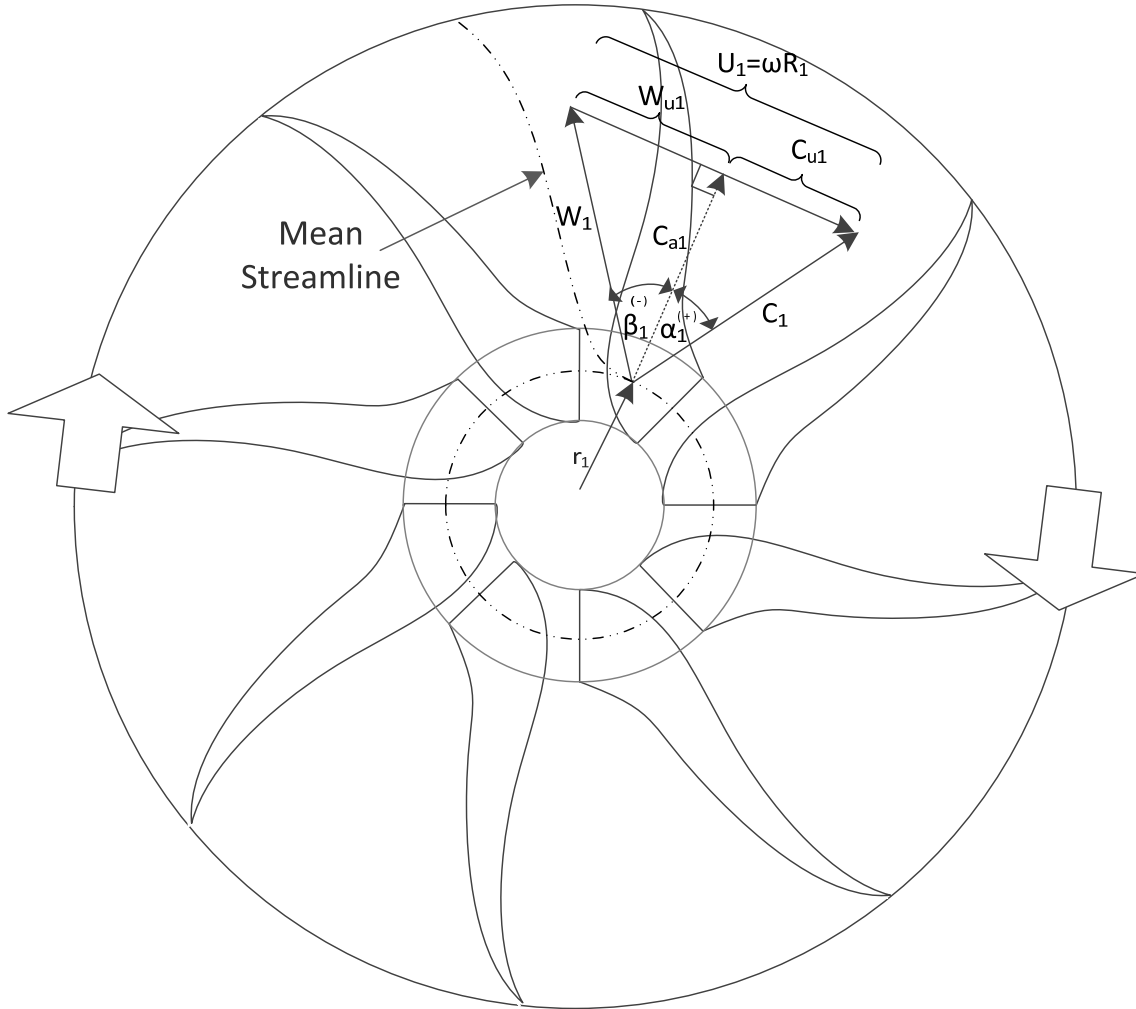


Figure 2.7: Impeller inlet velocity triangle.

Velocity triangles can also be drawn at the hub and shroud, the only difference will be the value of U_1 because the radius changes. From this, the Mach numbers at the hub, shroud and meanline can be determined using the speed of sound at the inlet (outputted by REFPROP from H_1 and S_1) and the relative velocities at each respective location.

2.3.2 Impeller Outlet

An estimated pressure ratio across the rotor is used to determine the ideal value of P_{02}

$$P_{02} = PR_{rotor} \times P_{01} \quad (2.6)$$

Next, by assuming an isentropic process, P_{02} and S_{02} (same as S_{01}) can be used to determine the ideal enthalpy at the rotor outlet ($H_{02,ideal}$) using REFPROP. From this, and the estimated rotor efficiency (which is updated later on) the actual enthalpy estimate at the rotor outlet can be obtained using

$$h_{02} = h_{01} + \frac{(h_{02,ideal} - h_{01})}{\eta_{rotor}} \quad (2.7)$$

The actual entropy estimate can be obtained from H_{02} , P_{02} , and REFPROP.

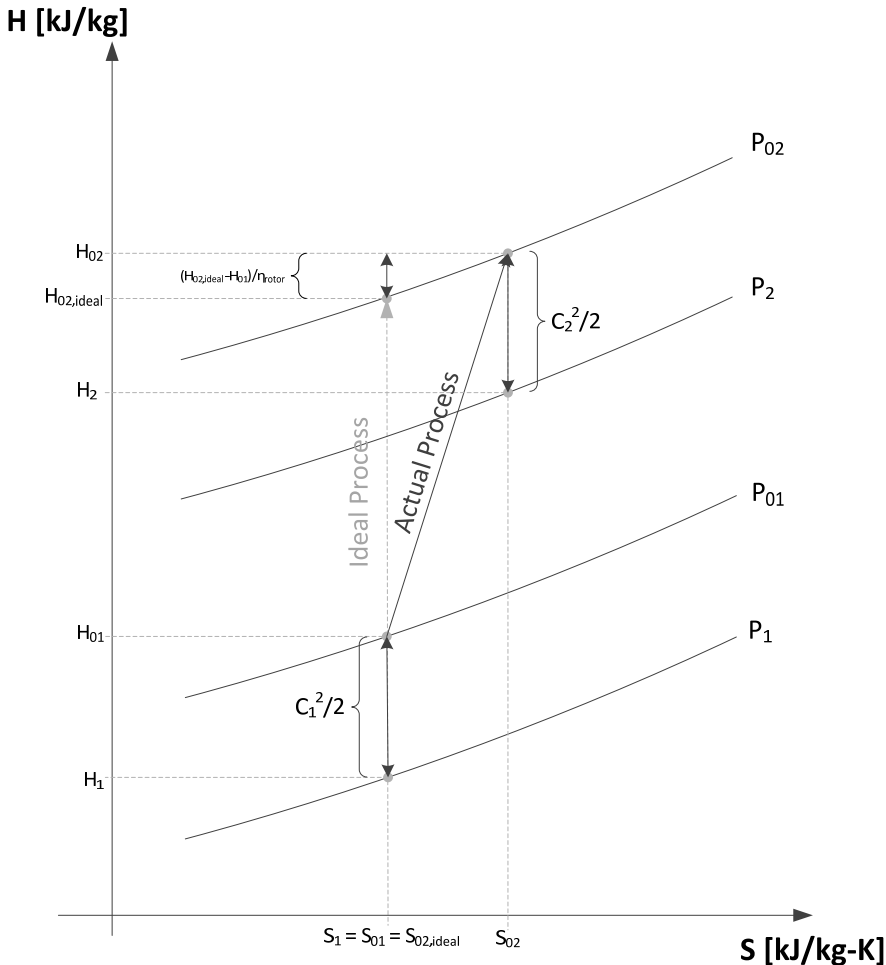


Figure 2.8: H-S Diagram at the rotor outlet (initial estimate).

Next, the static conditions are obtained using the conservation of mass given by

$$\dot{m} = \rho_2 A_2 C_{r2} \quad (2.8)$$

The area at the outlet of the impeller is defined as

$$A_2 = (2\pi r_2 - (Z_{full} + Z_{splitter})t_1)b_2 \quad (2.9)$$

There are still two unknowns left, however, from the Euler turbine equation 2.1 which can be re-written as

$$C_{U2} = \frac{h_{02} - h_{01} + U_1 C_{u1}}{U_2} \quad (2.10)$$

and knowing from trigonometry that

$$C_2 = \sqrt{(C_{U2})^2 + (C_{r2})^2} \quad (2.11)$$

The unknowns can be obtained using all the total conditions and iteration as follows:

- Use the total density as a first estimate for ρ_2
- Re-arrange equation 2.8 and solve for C_{r2}
- Compute Equation 2.11
- Compute the static enthalpy using an isentropic total-to-static process (Fig. 2.8)
- Call REFPROP with the static enthalpy and entropy to determine the ρ_2
- Update the first estimate of ρ_2 and continue this process until convergence

Now the values of C_2 , C_{r2} , U_2 (determined from the rotational speed) are known, so the full velocity triangle at the impeller outlet can be constructed using trigonometry as shown in Figure 2.9.

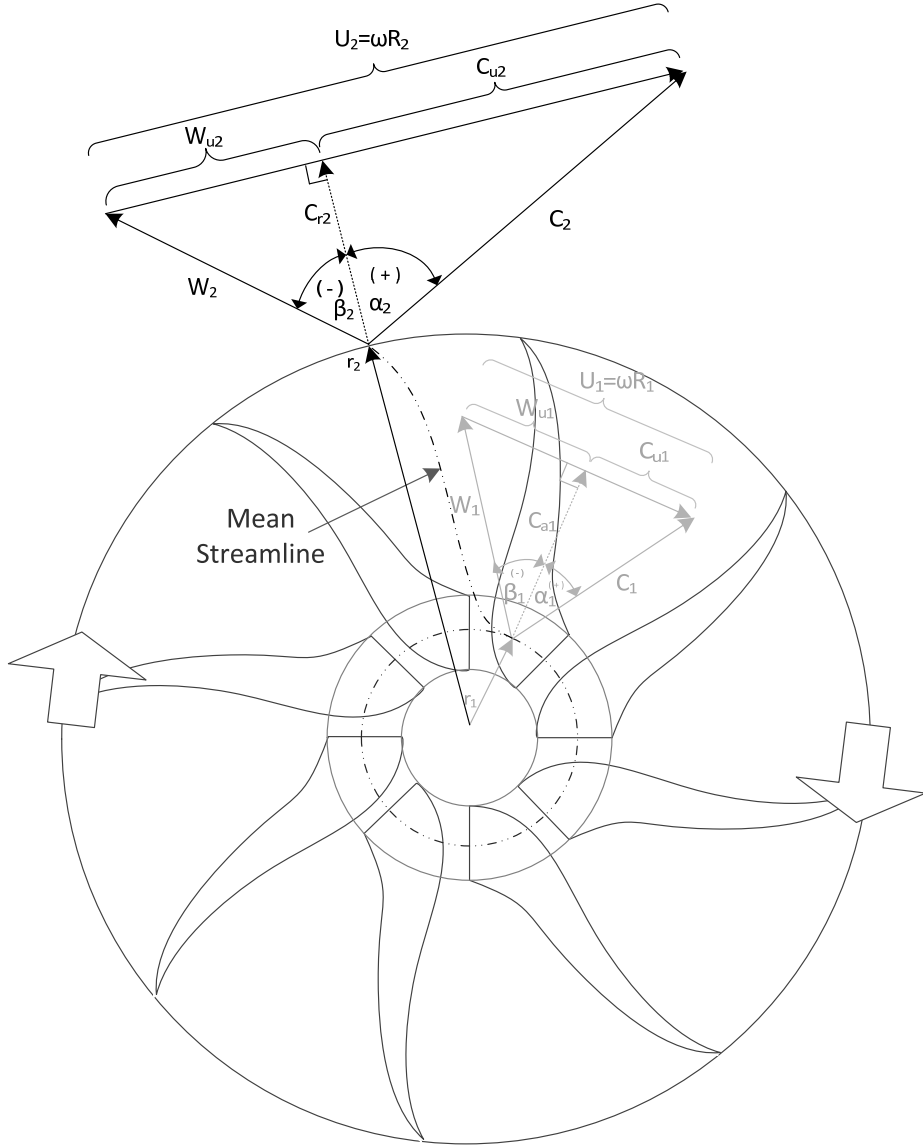


Figure 2.9: Rotor outlet velocity triangle.

With all thermodynamic properties and velocities at the inlet and outlet of the impeller now defined, it is possible to compute the loss correlations and achieve more accurate predictions of the impeller outlet conditions. Once these have been calculated, new values of H_{02} , S_{02} and the corresponding rotor efficiency are used to update the initial guesses. The new pressure ratio is used to update the estimated value in Equation 2.6, and this process continues until the target stage pressure ratio is achieved.

2.3.3 Internal Losses

This section provides the loss correlations which are used in the code. Oh et al.[2] performed a study on a range of loss correlations found in literature and determined an optimum set which are valid for a reasonable range of centrifugal compressors. This optimum set is presented below along with a description of each loss contribution.

2.3.3.1 Incidence Loss

Incidence losses occurs when the flow is misaligned with the actual metal angle at the impeller inlet. The incidence loss correction presented developed by Conrad et al. [7] is given as

$$\Delta h_{inc} = f_{inc} \frac{(W_{ui})^2}{2} \quad (2.12)$$

$$\text{where } f_{inc} = 0.5 - 0.7$$

However, a deviation was made from this loss correlation for the on-design Fortran code. At design point, it is desirable to design the metal angle such that the flow is aligned with it. For this reason, the incidence loss correction developed by Whitfield and Baines was used:

$$\Delta h_{inc} = \frac{\beta' - \beta_{opt}}{2} \quad (2.13)$$

In this equation, it is clear that the losses are a function of the actual misalignment angles, β' being the actual metal angle and β_{opt} being the metal angle where no misalignment occurs. This shows that for design point $\beta' = \beta_{opt}$ so there are no incidence losses.

2.3.3.2 Blade Loading Loss

Coppage et al. (1956) [8] developed a loss correlation for the blade loading loss given as

$$\Delta h_{BL} = 0.05 D_f^2 U_2^2 \quad (2.14)$$

D_f is the diffusion factor which provides a measure of the total deceleration of the flow as

$$D_f = 1 - \frac{W_2}{W_{1t}} + \frac{0.75 \Delta h / U_2^2}{(W_{1s}/W_2)[(Z/\pi)(1 - r_{1s}/r_2) + 2r_{1s}/r_2]} \quad (2.15)$$

and an estimate for the number of blades, Z , is provided by Aungier [3] as

$$Z = Z_{Full} + \frac{L_{Splitter}}{L_{Full}} Z_{Splitter} \quad (2.16)$$

The blade loading loss accounts for the momentum loss caused by boundary layers on the blade surfaces. Equation 2.15 is a function of the deceleration and turning of the flow in one-dimension. The first part determines the amount of diffusion through the passage, and the second term determines the loading distribution along the blade.

2.3.3.3 Skin Friction Loss

A correction factor for frictional losses of the flow at the wall surfaces was developed by Jansen (1967) as

$$\Delta h_{SF} = 2C_f \frac{L_b}{D_H} \bar{W}^2 \quad (2.17)$$

where \bar{W} is the mean relative velocity through the impeller passage given by

$$\bar{W} = \frac{C_{1s} + C_2 + W_{1s} + 2W_{1h} + 3W_2}{8} \quad (2.18)$$

the skin friction is assumed to equal to a fully developed flow in a pipe of circular cross-section. The length of the impeller passage is determined using equation 2.3 and the diameter of the equivalent pipe corresponds to the average hydraulic diameter, which is determined as the average of the throat and tip values as

$$D_H = \frac{4(CrossSectionalArea)}{WettedPerimeter} \quad (2.19)$$

The Reynolds number needed for the skin friction calculation is obtained from

$$Re_{dH} = \frac{\bar{\rho} \bar{W} D_H}{\mu} \quad (2.20)$$

Where $\bar{\rho}$ is the average static density of the impeller inlet and outlet. Viscosity, μ , at the impeller inlet and outlet are obtained using the REFPROP transport subroutines. These values are then averaged.

2.3.3.4 Clearance Loss

A small gap between the stationary casing and the impeller is inevitable. This will cause fluid to leak from the high pressure side to the low pressure side of the blade and cause leakage losses. A correction factor was developed by Jansen [9] and is

defined as

$$\Delta h_{cl} = 0.6 \frac{\varepsilon}{b_2} C_{U2} \sqrt{\frac{4\pi}{b_2 Z} \left[\frac{r_{1t}^2 - r_{1h}^2}{(r_2 - r_{1t})(1 + \frac{\rho_2}{\rho_1})} \right] C_{U2} C_{a1}} \quad (2.21)$$

The flow is assumed to undergo a sudden contraction and sudden expansion when passing through the clearance gap. Equation 2.21 is obtained by applying a standard loss factor to the sudden contraction and expansion process, and assuming an ideal loading distribution to estimate the pressure difference across the clearance gap.

2.3.3.5 Mixing Loss

Mixing losses occur because of the finite thickness of the blade at the outlet which result in non-uniform flow velocities at the impeller outlet.

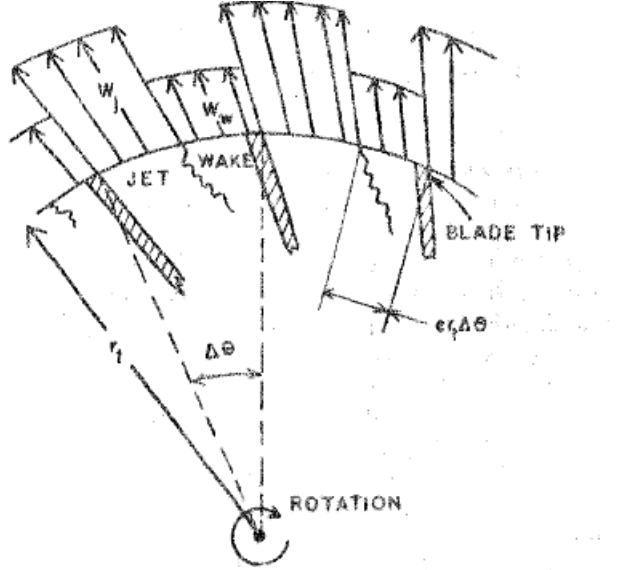


Figure 2.10: Non-uniform velocities at impeller outlet (Johnston and Dean, 1966).

An abrupt expansion loss is used to reasonably predict the mixing losses and is provided by Johnston and Dean (1966) [10] as

$$\Delta h_{mix} = \frac{1}{1 + \tan^2 \alpha_2} \left(\frac{1 - \varepsilon_{wake} - b_3/b_2}{1 - \varepsilon_{wake}} \right)^2 \frac{C_2^2}{2} \quad (2.22)$$

where ε_{wake} is the wake fraction of the blade-to-blade spacing estimated from the velocities before and after the mixing. The wake can be estimated from the diffusion factor given by (Lieblein, 1959)

$$D_{eq} = \frac{W_1 + W_2 + 2\pi D_2 \frac{U_2 C_{U2} - U_1 C_{U1}}{U_2 Z L_b}}{2} \quad (2.23)$$

And the velocity at which separation occurs:

$$\begin{aligned} W_{sep} &= W_2; & D_{eq} &\leq 2 \\ W_{sep} &= W_2 \frac{D_{eq}}{2}; & D_{eq} &> 2 \end{aligned} \quad (2.24)$$

It is assumed that the wake mixing loss involves no significant tangential component of velocity because the wake mixing occurs after the impeller (where no blade forces are present). So the meridional velocities can be estimated using

$$\begin{aligned} C_{m,wake} &= \sqrt{W_{sep}^2 - W_U^2} \\ C_{m,mix} &= \frac{C_{m2} A_2}{\pi D_2 b_2} \end{aligned} \quad (2.25)$$

Finally, the estimate for the wake fraction needed to solve equation 2.22 is given as

$$\varepsilon_{wake} = 1 - \frac{C_{m,wake}}{C_{m,mix}} \quad (2.26)$$

2.3.3.6 Updating The Performance Prediction

Once the losses have all been calculated, an updated value of the total enthalpy can be obtained by adding the calculated losses to the ideal total enthalpy as

$$h_{02} = h_{02,ideal} + \Delta h_{inc} + \Delta h_{BL} + \Delta h_{SF} + \Delta h_{cl} + \Delta h_{mix} \quad (2.27)$$

and the updated rotor efficiency is given as

$$\eta_{rotor} = \frac{h_{02,ideal} - h_{01}}{h_{02,real} - h_{01}} \quad (2.28)$$

which is then used update the estimate used in equation 2.7, and this process is repeated until the efficiency (and therefore entropy) converges.

2.3.4 Slip Factor

The impeller outlet velocity triangle previously calculated was determined by assuming that the relative flow, W_2 , is in the direction of the blade metal angle at

the outlet, β_2 . Because of the phenomenon of slip which was argued by Stodola (1927), this will not be the case. A correction factor for this was developed by Stodola and later refined by Wiesner and Busemann (1967) which is given by

$$\sigma = 1 - \frac{\sqrt{\sin\beta_2} \sin\alpha_2}{Z^{0.7}} = \frac{C_{U2}}{C_{U2,(\beta_2=\beta'_2)}} \quad (2.29)$$

The slip factor remains constant for most cases. However, for cases where the mean radius ratio ϵ_{LIM} is past a certain limit, the slip factor is corrected by

$$\sigma_{corr} = \sigma \left(1 - \frac{\epsilon - \epsilon_{LIM}}{1 - \epsilon_{LIM}} \right)^{\sqrt{\frac{\beta_2}{10}}} \quad (2.30)$$

and the limiting mean radius ratio is given by

$$\epsilon_{LIM} = \frac{\sigma - \sigma^*}{1 - \sigma} \quad (2.31)$$

where

$$\sigma^* = \sin(37^\circ + \beta_2) \quad (2.32)$$

This results in an updated velocity triangle, using the value of the slip factor which is defined as the ratio of the actual discharge radial velocity to the ideal radial velocity if no slip were present given by equation 2.29.

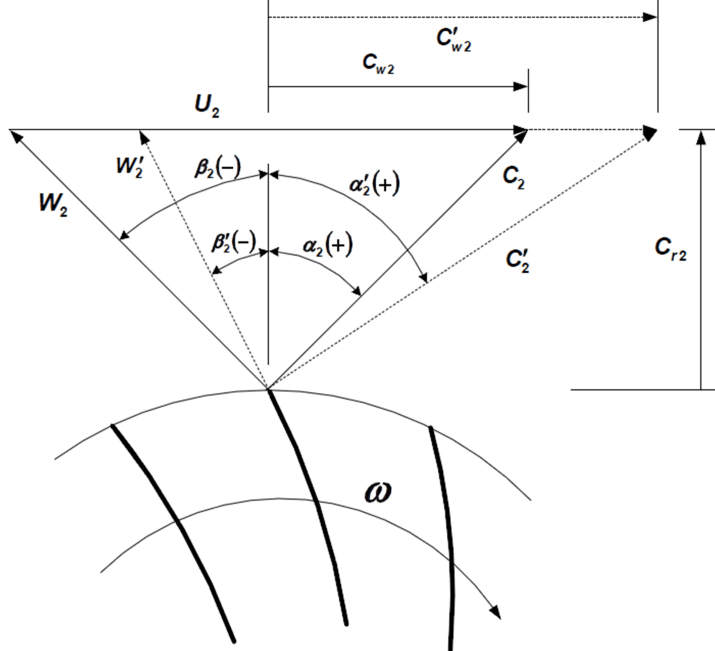


Figure 2.11: Impeller outlet velocity triangle with slip (Sjolander,[4]).

2.3.5 Parasitic Losses

Parasitic losses account extra work required to drive the compressor. They do not affect the flow thermodynamic conditions so they are added in after the previous iteration. They account for disc friction work, leakage work, and recirculation work.

2.3.5.1 Disc Friction Loss

Since the rotating impeller is enclosed inside some fluid filled enclosure, unless it is operating inside a vacuum, the disc will experience a frictional force which introduces losses. Daily and Nece [11] conducted an experiment to determine the losses caused by a smooth plane disc enclosed within a right-cylindrical chamber. These models are used to determine the similar disc friction losses in centrifugal compressors as

$$\Delta h_{DF} = f_{DF} \frac{\bar{\rho} r_2^2 U_2^3}{4\dot{m}} \quad (2.33)$$

where the friction factor is given by

$$f_{DF} = \begin{cases} \frac{2.67}{Re_{DF}^{0.5}} & , \quad Re_{DF} < 3 \times 10^5 \\ \frac{0.0622}{Re_{DF}^{0.2}} & , \quad Re_{DF} \geq 3 \times 10^5 \end{cases} \quad (2.34)$$

and the Reynolds number can be determined as

$$Re_{DF} = \frac{U_2 r_2}{v_2} \quad (2.35)$$

2.3.5.2 Recirculation Loss

Depending on the value of α_2 , flow will begin to recirculate back into the impeller section after leaving the impeller outlet. This will result in flow being recompressed, and energy will be wasted. Oh et al. provides a method for estimating this loss with the following

$$\Delta h_{RC} = 8.0 \times 10^{-5} \sinh(3.5\alpha_2^3) D_f^2 U_2^2 \quad (2.36)$$

where D_f can be obtained from equation 2.15.

2.3.5.3 Leakage Loss

Some of the flow exiting the impeller gets leaked through the seals and into the casings due to pressure differences. A loss correction for the leakage losses is provided by Aungier (2000) [3].

$$\Delta h_{LL} = \frac{\dot{m}_{LL} U_{LL} U_2}{2\dot{m}} \quad (2.37)$$

where the velocity of the clearance gap flow is given by

$$U_{LL} = 0.816 \sqrt{\frac{2\Delta P_{LL}}{\rho_2}} \quad (2.38)$$

The average pressure difference across the gap is determined by

$$\Delta P_{LL} = \frac{\dot{m}(r_2 C_{U2} - r_1 C_{U1})}{Z \left(\frac{r_1 + r_2}{2} \right) \left(\frac{b_1 + b_2}{2} \right) L_b} \quad (2.39)$$

Lastly, the blade clearance gap leakage flow rate can be given by

$$\dot{m}_{LL} = \rho_2 Z s L_b U_{LL} \quad (2.40)$$

where s is the clearance gap width, equation 2.37 can be solved using equations 2.38, 2.39, and 2.40.

2.3.5.4 Updating the Performance Prediction

With the parasitic losses now calculated, the entropy increase caused by them can be added to the analysis and the diffuser inlet total enthalpy can be estimated.

$$h_{03} = h_{02} + \Delta h_{DF} + \Delta h_{RC} + \Delta h_{LL} \quad (2.41)$$

2.3.6 Diffuser Losses

As mentioned before, the diffuser analysis is not of primary importance at this stage in the Gas Turbine Project. A loss factor for a vaneless diffuser was suggested in Oh et al. however, an ideal gas assumption was made and therefore can not be used. For this reason, a simple diffuser loss factor κ_D is input by the user and applied to the total pressure resulting in the diffuser outlet conditions. This is usually given by

$$P_{04} = P_{03} - \kappa_D \left(\frac{1}{2} \rho C_3^2 \right)$$

or extending this to account for compressibility effects

$$P_{04} = P_{03} - \kappa_D (P_{03} - P_3) \quad (2.42)$$

There are several published data for reasonable values of κ_D as a function of non-

dimensionalized compressor performance parameters available. The values κ_D can be obtained from literature, Zhu and Sjolander (1987) [12], Johnston and Dean (1966) [10], or varied and set as a design target for when the diffuser is being designed. Typical values range from 0.01 to 0.4 for extreme cases.

2.3.7 Volute Losses

It is first assumed that the total conditions at the diffuser outlet are equal to the conditions at the volute inlet. Next, a similar method is employed in the volute as was done in the diffuser analysis.

$$P_{06} = P_{05} - \kappa_V(P_{05} - P_5) \quad (2.43)$$

The value for κ_V can be obtained similarly through either literature, or set as a design target for volute design. Typically, the loss factors of the volute will be less than the diffuser and range from 0.01 to 0.2.

2.3.8 Compressor Outlet of Performance Prediction

Since the diffuser and volute are both stationary, it is assumed that no additional energy is added to the fluid after the impeller outlet. Therefore,

$$h_{02} = h_{03} = h_{04} = h_{05} = h_{06} \quad (2.44)$$

Inputting the values obtained from equations 2.43 and 2.44 into REFPROP, all other thermodynamic properties at the compressor outlet can then be determined. The new total-to-total stage pressure ratio is determined and compared with the target pressure ratio. If it is close enough to the target, the analysis is complete, otherwise it will correct the rotor pressure ratio estimate (equation 2.6) using

$$PR_{rotor} = PR_{rotor} \left(\frac{Target_{PR}}{PR_{stage}} \right)$$

The entire process is repeated until the target stage pressure ratio is met.

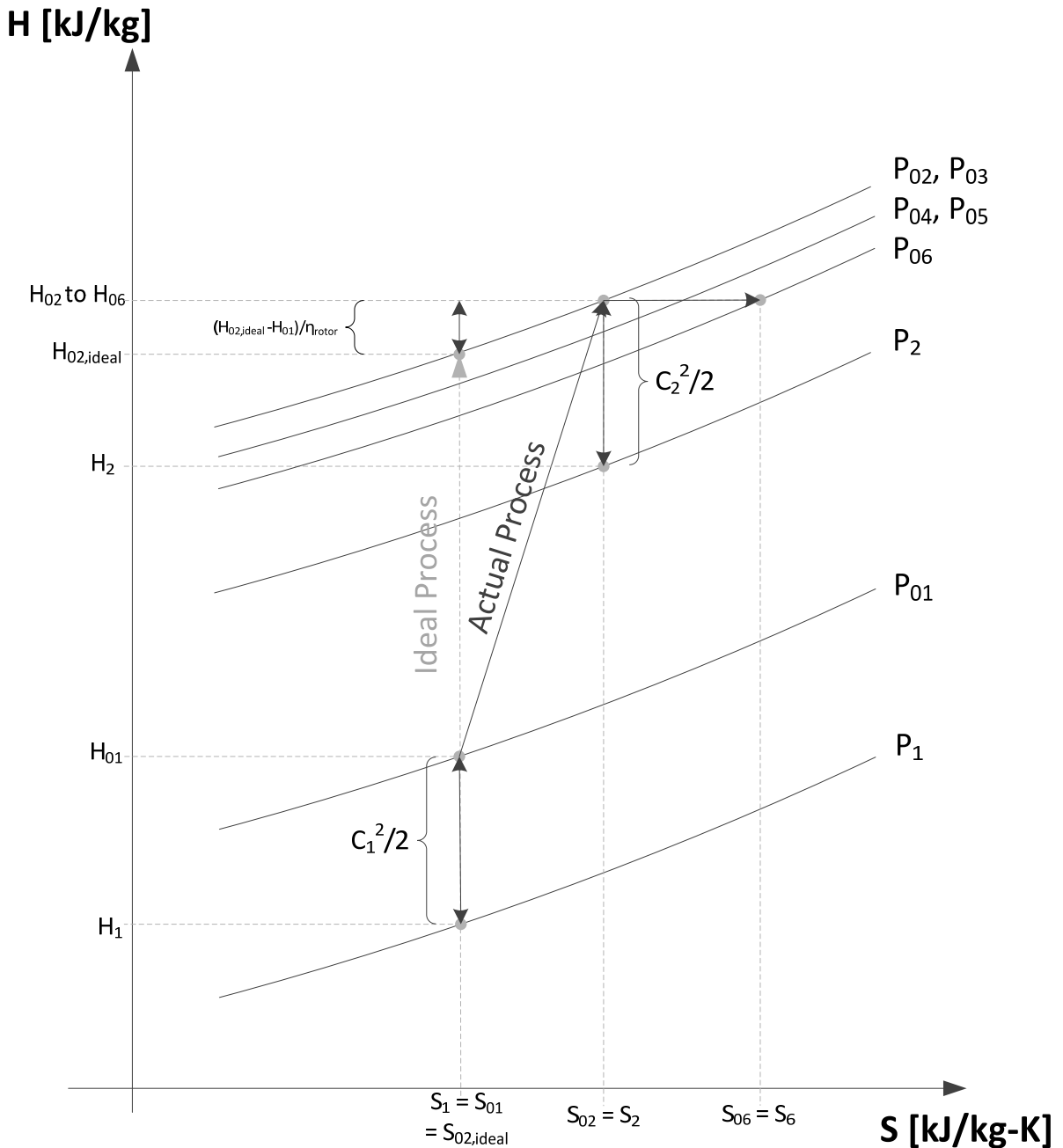


Figure 2.12: Full compressor performance H-S diagram.

Section 3

Results

This section provides information on the accuracy of the centrifugal compressor meanline analysis program. The computer program predictions are compared with experimental data obtained for the Eckardt O-Rotor by Eckardt (1975) [13].

3.1 CCMD Benchmark Testing

The Eckardt O-Rotor was one of three rotors analysed by Eckardt in the 70's. Since then, it has been used as a benchmark case for centrifugal impeller analysis by many researchers. For this reason it was chosen as a suitable benchmark test case for the CCMD code.

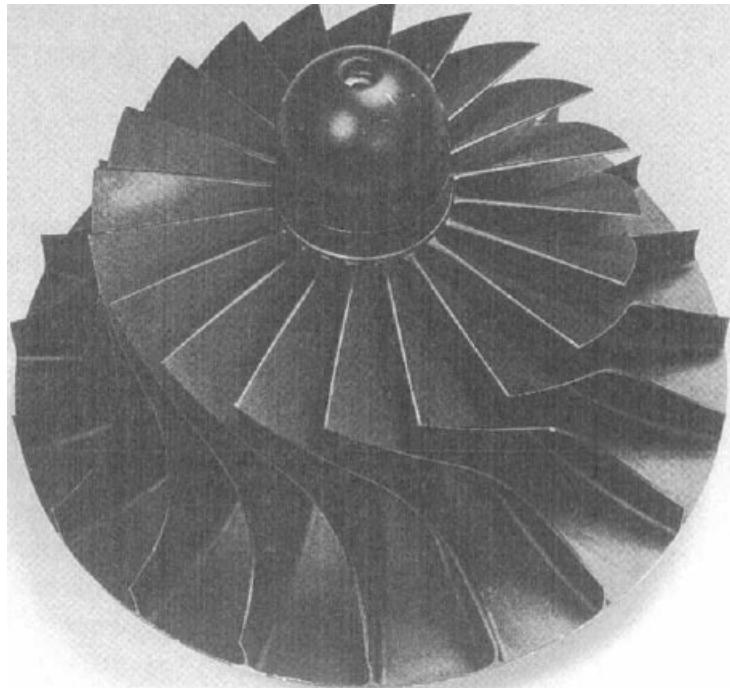


Figure 3.1: The Eckardt O-Rotor (Japikse and Baines, 1997).

The dimensions for the rotor were obtained from a recent study done by de Wet (2011) and are shown in Table 3.1.

Table 3.1: Eckardt O-Rotor Dimensions

Location	Dimension	Value
Inlet	r_{1h} (mm)	45
	r_1 (mm)	103.99
	b_1 (mm)	95
	t_{b1} (mm)	2.11
	β_{1h} (deg)	57.12
	β_1 (deg)	33.83
	β_{1s} (deg)	26.75
	α_1 (deg)	1.68
Outlet	r_2 (mm)	200
	b_2 (mm)	26
	t_{b2} (mm)	1.08
	α_2 (deg)	86.15
	β_2 (deg)	89.78
Misc.	L_B (mm)	202.26
	L_{FB} (mm)	171.26
	Z	20
	s_{CL} (mm)	0.372

These needed values were taken from Table 3.1 and input into the centrifugal compressor meanline design code (CCMD). The target pressure ratio was set to 2.094 for a rotational speed of 14000 RPM and 5.31 kg/s at optimum efficiency (design point) which was specified in de Wet [14] (From Japikse and Baines, 1997). Since only the impeller was being analyzed, the diffuser and volute loss factors were set to zero and the program was run. Also, the inlet conditions to the impeller were at atmospheric ($T_{01} = 288K$ and $P_{01} = 101.325kPa$).

Table 3.2: Eckardt O-Rotor Performance. CCMD vs. Experimental Data

	Experiment	CCMD	Error
T_{02} (K)	363.5	365.0	0.41 %
P_{02} (kPa)	220.5	212.2	-3.76 %
P_2 (kPa)	144.7	139.7	-3.46 %
β_{1h} (deg)	57.12	51.76	5.36°
β_1 (deg)	33.83	28.27	5.56°
β_{1s} (deg)	26.75	21.69	5.06°
β_2 (deg)	89.78	82.29	7.49°
α_2 (deg)	66.3	68.5	2.2°
η_{stage}	88%	88.5 %	0.5%

The outlet thermodynamic conditions were predicted with less than 4% error from

those measured experimentally. Also, the flow velocities at the inlet and outlet were predicted to be within less than 7.5 degrees of the actual metal angles. Since the simulated condition was assumed to be at design point, the flow angles should be aligned very closely to the metal angle to minimize losses and this was predicted reasonably by CCMD.

Section 4

Conclusion

The idea of operating centrifugal compressors near the critical point to reduce compression work is only just beginning to emerge in industrial applications, there remains lots of potential for improving the engineering and design methods which are, or will be used. That being said, there still remains lots of ways of imporving the CCMD code as well as using it for the Gas Turbine Project for compressor design.

4.1 Recommendations

Firstly, it is recommended to research and find experimental data of supercritical fluids near the critical point operating in centrifugal compressors. This can be used to validate the accuracy of the meanline code near the critical point which is of primary importance. An alternative method would be to simulate a non-ideal flow near the critical point and compare the results to the CCMD prediction.

Once experimental data is obtained, it will become possible to investigate the validity of several assumptions that were made. They did not have much effect in the ideal gas region, however they may be significant sources of error in near the critical point. The first assumption was taking the average viscosity at the inlet and outlet of the rotor for the skin friction loss correction factor, and may have significant error when viscosity changes are highly non-linear.

Another assumption was made when estimating the wake velocities in the mixing loss correlation provided by Aungier. The meridional velocities were estimated from the separation velocity and conservation of momentum, and in order to do this, the gas density was assumed to be approximately constant, and should therefore be investigated. Similarly, the derivation for the velocity of leakage loss (see equation 2.38) was assumed to be constant density as well.

4.2 Final Remarks

The meanline analysis method once again proved to provide reasonably accurate performance results when compared with experimental data in the ideal gas region and can be used for preliminary design stages of centrifugal compressors. What would take weeks of setting up a simulations on commercial CFD packages, is reduced to seconds of just a few clicks and changing variables. CCMD will hopefully provide future students on the Gas Turbine Project with a method for estimating an optimal geometry to be used on the plant. The CCMD program can be obtained free of charge by emailing the author at sukhveersanghera@cmail.carleton.ca.

References

- [1] Dostal, V., Driscoll, M.J., and Hejzlar, P. A Supercritical Carbon Dioxide Cycle for Next Generation Nuclear Reactors. Massachusetts Institute of Technology, Cambridge, Massachusetts. March 10, 2004. 2
- [2] Oh, H.W., Yoon, E.S., and Chung, M.K. An Optimum Set of Loss Models for Performance Prediction of Centrifugal Compressors. Proceedings of the Institution of Mechanical Engineers, Volume 211, 1997. pp. 331 - 338. 3, 14
- [3] Aungier, Ronald H. Centrifugal Compressors: A Strategy for Aerodynamic Design and Analysis. ASME Press, 2000. 3, 15, 19
- [4] Sjolander, S.A. MECH 5401 Supplementary Notes. Department of Mechanical and Aerospace Engineering. Carleton University, Ottawa, Ontario, Winter 2013. vi, 6, 10, 18
- [5] E.W. Lemmon, and M.L. Huber NIST REFPROP: Version 9.0. Available: <http://www.nist.gov/srd/nist23.cfm>. Last updated: February 22, 2013. 3, 7
- [6] Urieli, I. Thermodynamics Chapter 2 Notes, Ideal gas equation of state. http://www.ohio.edu/mechanical/thermo/Intro/Chapt.1_6/Chapter2b.html. Accessed: March 18th, 2013. vi, 7
- [7] Conrad, O., Raif, K. and Wessels, M. The calculation of performance maps for centrifugal compressors with vaneless diffusers. ASME 25th Annual International Engineering Conference and 25th Annual Fluids Engineering Conference on Performance Prediction of Centrifugal Pumps and Compressors, New Orleans, Louisiana, March 1980. pp. 135-147. 14
- [8] Coppage, J.E., Dallenbach, F., Eichenberger, H.P., Hlavaka, G.E., Knoernschild, E.M. and Van Lee, N. Study of supersonic radial compressors for refrigeration and pressurization systems. WADC report 55-257, 1956. 14
- [9] Jansen, W. A method for calculating the flow in a centrifugal impeller when entropy gradients are present. Royal Society Conference on Internal Aerodynamics (Turbomachinery), 1967 (IME). 15
- [10] Johnston, J.P. and Dean Jr., R.C. Losses in vaneless diffusers of centrifugal compressors and pumps. Analysis, experiment and design. Trans. ASME, Journal of Engineering for Power, 1966, 88, 49-62. 16, 21

- [11] Daily, J. W. and Nece, R.E. Chamber dimension effects on induced flow and frictional resistance of enclosed rotating disks. Trans. ASME, Journal of Basic Engineering, 1960, 82, 217-232. 19
- [12] Y. Zhu and S.A. Sjolander. Effect of Geometry on the Performance of Radial Vaneless Diffusers. Journal of Turbomachinery, 1987, Volume 109, Issue 4, 550-556. 21
- [13] Eckardt, D. Flow Field Analysis of Radial and Backswept Centrifugal Compressor Impellers. Part I: Flow Measurements using a Laser Velocimeter. Performance Prediction of Centrifugal Pumps and Compressors. ASME pp. 77-86. 23
- [14] De Wet, A.L. Performance Investigation of a Turbocharger Compressor. Department of Mechanical and Mechatronic Engineering Master of Science Thesis. University of Stellenbosch, South Africa, 2011.

24